JACS
JOURNAL OF THE AMERICAN CHEMICAL SOCIETY
pubs.acs.org/JACS
Article

Subcellular Photocatalysis Enables Tumor-Targeted Inhibition of Thioredoxin Reductase I by Organogold(I) Complexes

Moyi Liu, Haitao Liu, Yan Yang, Xiaolin Xiong,* and Taotao Zou*

Cite This: J. Am. Chem. Soc. 2025, 147, 15719−15731
Read Online

ABSTRACT: Selective inhibition of TrxR1 over TrxR2 is a highly sought-after goal, because the two enzymes play distinct roles in cancer progression. However, achieving targeted inhibition is challenging due to their high homology and identical active site sequence. Herein we report a new subcellular photocatalysis approach for targeted inhibition by controllably activating organogold(I) prodrugs within the cytosol, the exclusive location of TrxR1. The NHC-Au(I)-alkynyl complexes are stable and evenly distributed in the cell; they can meanwhile be efficiently transformed into active NHC-Au(I)-L species (L = labile ligands) via a radical mechanism by photocatalysts released into the cytosol (from endosome/lysosome) upon light irradiation, leading to selective inhibition of TrxR1 without affecting TrxR2. This results in strong cytotoxicity to cancer cells with much higher selectivity than auranofin, a pan TrxR inhibitor that cannot discriminate TrxR1/2, along with potent antitumor activities in multiple zebrafish and mouse models. This subcellular prodrug activation may thus suggest a novel approach to precision targeting using the remarkable spatial control of photocatalysis.

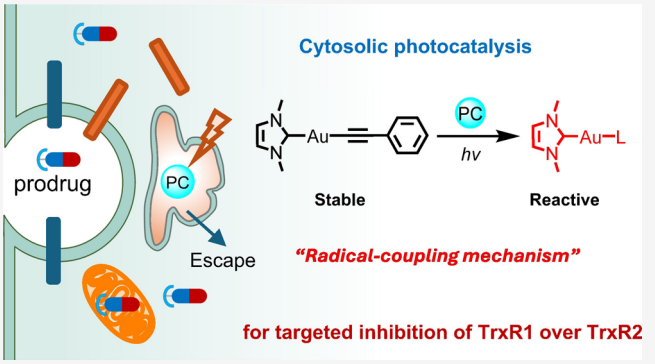

INTRODUCTION

Living organisms are constantly exposed to an oxidative environment, giving a myriad of oxidation reactions within our body.[1,2] To counter oxidative stress, living systems have evolved essential antioxidizing mechanisms to maintain redox homeostasis.[3] Among them, the thioredoxin system is ubiquitous and plays a crucial role in keeping the redox states of proteins. Thioredoxin reductase (TrxR) is the sole enzyme in this system responsible for catalyzing the NADPH-dependent reduction of thioredoxin, facilitating the downstream reduction of protein disulfide bonds.[4] Due to its regulatory role that is potentially associated with cancer, TrxR has been considered as a promising therapeutic target.[5] In past years, tremendous endeavors have been dedicated to developing TrxR inhibitors, with gold complexes being among the most widely investigated types of compounds.[6−18] In particular, gold(I) complexes with N-heterocyclic carbene (NHC),[19−32] alkynyl,[33−37] phosphine,[38−42] thiolate,[43−46] and others[47−54] have been extensively studied, and some of them display low nanomolar or even picomolar inhibition activities toward purified enzymes, with quite a few notable examples display antitumor activities in vivo.

Nevertheless, humans generally express two isoforms of TrxR throughout the body: TrxR1, located in the cytosol, and TrxR2, found in the mitochondria.[55,56] While both isoforms are essential, they have distinct roles in cancer progression. For example, in cancer patients of kidney renal papillary cell carcinoma (KIRP), high TrxR1 expression is linked to poor survival outcomes, i.e., a 5-year survival rate of 44% in high expression groups, compared to 83% in low expression groups, $p = 7.1 \times 10^{-7}$ (Figure 1a(i), upper panel, and Table S1), whereas those with elevated levels of TrxR2 have significantly higher 5-year survival rates (80% for high expression groups versus 51% for low expression groups, $p = 6 \times 10^{-6}$, Figure 1a(i), lower panel, and Table S1). Similar opposite correlations were found in patients with colorectal adenocarcinoma (Figure 1a(ii), ovarian cancer (Figure 1a(iii), lung adenocarcinoma (Figure 1a(iv), and others (Table S1). Furthermore, CRISPR knockout studies involving 1152 cancer cell lines show that loss of *TXNRD1* (encoding TrxR1) significantly impacts the proliferation of most cancer cells (Figure 1b), highlighting TrxR1 as a potential anticancer target. In contrast, knockout of *TXNRD2* does not significantly affect cell growth (Figure 1b), suggesting that TrxR2 plays a different role. In addition, although human tumor tissues generally display moderate-to-strong TrxR1 staining, the staining intensity of TrxR2 is variable (Figure 1c). Together with the protecting role of TrxR2 in numerous normal tissues,[57−60] it could be concluded

Received: February 20, 2025
Revised: March 19, 2025
Accepted: April 11, 2025
Published: April 24, 2025

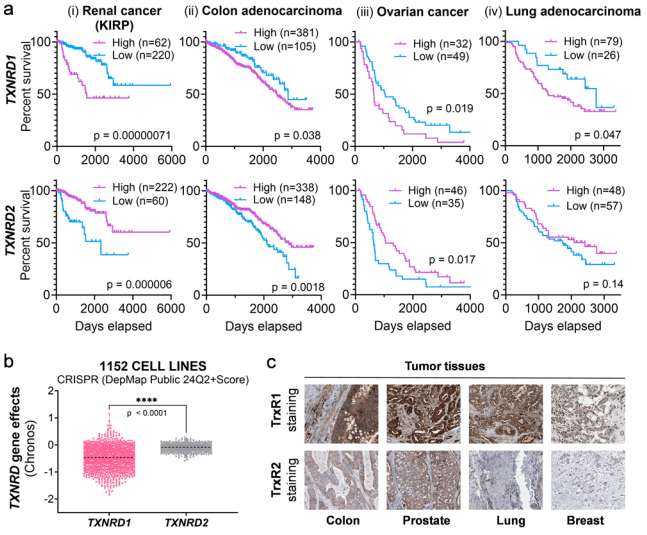

Figure 1. Pathological analysis and gene effects of the two isoforms of TrxR in cancer progression. (a) Survival of human patients of kidney renal papillary cell carcinoma (KIRP), colon adenocarcinoma, ovarian cancer and lung adenocarcinoma with high or low expression of *TXNRD1* or *TXNRD2* gene. Data were reproduced from *The Human Protein Atlas*.[61,62] (b) Proliferation of cancer cells upon CRISPR knockout of the *TXNRD1* or *TXNRD2* gene. Chronos is an algorithm designed to infer the fitness effects of gene knockouts. In this system, a value of 0 indicates that a gene is nonessential for cellular proliferation, while values approaching −1 signify that the gene is essential for growth/survival. Data were from *The Cancer Dependency Map*.[63] (c) Representative staining images of TrxR1 and TrxR2 of tumor tissues from human patients. Data were obtained from *The Human Protein Atlas*.

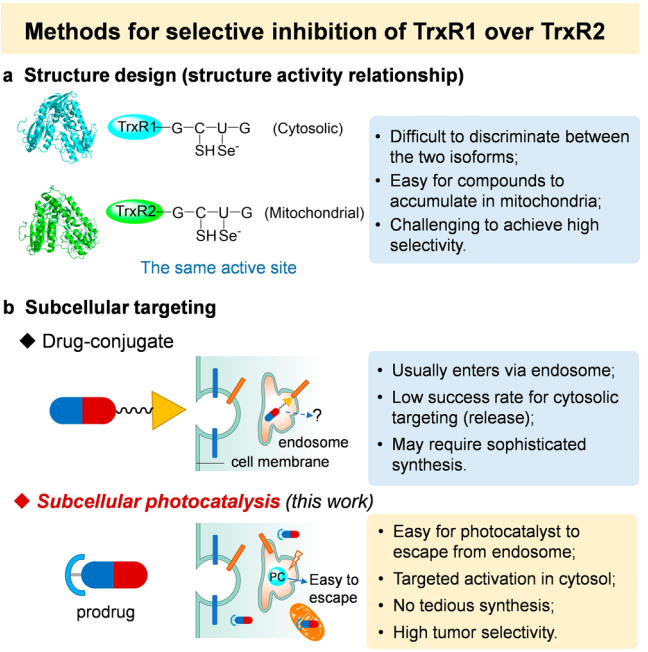

Figure 2. Approaches for targeted inhibition of TrxR1 over TrxR2: (a) Conventional design based on structure−activity optimization, which poses challenges due to the high similarity between the active sites of TrxR1 and TrxR2; (b) subcellular targeting strategies, including small molecule-drug conjugates that often lead to endosomal trapping and subcellular photocatalysis, which allows for selective TrxR1 inhibition through targeted cytosolic prodrug activation (PC = photocatalyst).

that while targeting TrxR1 could offer therapeutic benefits, care must be taken with TrxR2. The latter mitochondrial isoform does not appear to be associated with cancer proliferation, and its inhibition might compromise anticancer efficacy while potentially inducing toxicity in normal tissues. These differential roles underscore the complexity of redox regulation in cancer and emphasize the need for precise therapeutic strategies.

While TrxR1 and TrxR2 are encoded by separate genes, the two isoforms exhibit high homology and share an identical catalytic active site sequence (Gly-Cys-Sec-Gly, Figure 2a).[55] The presence of a nucleophilic thiol (R-SH) adjacent to a more nucleophilic selenol (R-Se$^-$) allows TrxR to be inhibited by various electrophiles, including both organic and inorganic small molecules. Notably, increasing examples of gold complexes have been identified that potently inhibited TrxR rather than the analogous glutathione reductase, which lacks selenocysteine.[64] However, these gold complexes show limited selectivity in discriminating cytosolic TrxR1 from mitochondrial TrxR2, with many preferentially accumulating in mitochondria.[12,18,64,65] This would unavoidably damage TrxR2 and cause undesirable side effects. On the other hand, the distinct localization of TrxR1 and TrxR2 offers a potential strategy for differentiating between the two enzymes through subcellular targeting (Figure 2b).[66] However, lipophilic compounds tend to accumulate in mitochondria, while hydrophilic compounds, such as those conjugated with cytosol-targeting peptides, are typically trapped in endosomes and only exceptional cases can escape into cytosol.[66−68] It remains a big challenge to controllably deliver inhibitors into the cytosol to enable selective cancer targeting.

In the literature, it is known that light displays a high spatiotemporal selectivity, with notable examples of photodynamic therapy (PDT),[69−72] which has been clinically used for cancer treatment, and photoactivated chemotherapy (PACT),[73−77] which facilitates targeted drug release.[78−105] Of note, while hydrophilic photosensitizers, such as rose bengal (RB), and methylene blue (MB), enter cancer cells via endocytosis and accumulate in endosome/lysosome,[106−110] they can readily escape into cytosol upon irradiation by a noncytotoxic dose of light.[66,111−114] In view of the robust proximity control of photocatalysis in living systems,[115−119] we conceive the possibility of using photocatalysis to control the subcellular activation of gold prodrugs for targeted TrxR1 inhibition. Herein we report a subcellular photocatalysis strategy to controllably activate gold(I) prodrugs within the cytosol but not mitochondria for selective inhibition of TrxR1. The NHC-Au(I)-alkynyl complexes we developed are stable against thiols under buffer conditions[37] and are evenly distributed in the cell; upon light irradiation, they can be selectively transformed into reactive NHC-Au(I)-L (L = labile ligands) species by catalytic amount of RB or MB within the cytosolic region, leading to potent inhibition of TrxR1 over TrxR2, and strong cytotoxicity toward cancer cells but not the normal ones under both in vitro and in vivo conditions. To the best of our knowledge, this represents the first example of utilizing subcellular photocatalytic activation to achieve discriminative inhibition of tumor isoform targets.

https://doi.org/10.1021/jacs.5c03186
J. Am. Chem. Soc. 2025, 147, 15719−15731

RESULTS AND DISCUSSION

Organogold(I) Is Photocatalytically Activatable through a Radical-Bimolecular Reductive Elimination Process. At first, a robust photocatalysis system needs to be developed. We focused on the previously reported NHC-Au(I)- alkynyl complexes since they display high thiol-stability before activation.[37] However, bioorthogonal activation by palladium(II) appears to suffer low activity in the presence of physiological thiols. So, we checked whether these complexes can be photocatalytically activated and if such a strategy can improve the activation efficiency. We prepared **1a** and its analogues **1a′** and **1b**−**1g**, in accordance with the literature procedure (Figure 3, upper panel, see characterization data in the Supporting Information). These complexes are soluble (>10 mM) in organic solvents such as CH_2Cl_2, CH_3CN, DMF, and DMSO. These organogold(I) complexes were dissolved in DMSO (as 10 mM stocks) and then diluted in aqueous solution for characterization of reactivity and the biological studies, unless otherwise noted.

We screened the commonly used photocatalysts including Eosin Y (EY), RB, MB, $[Ru(bpy)_3]Cl_2$, and $[Ir(ppy)_2bpy]Cl$ (where bpy = 2,6-bipyridine and Hppy = 2-phyenylpyridine; the structures of the former three photocatalysts are shown in Figure 3, upper panel). Probe-1, a nonemissive coumarin precursor that can be selectively converted into fluorescent coumarin only by active Au(I) species but not **1a**, was used to examine their activities (Figure 3, lower panel inset, and Figure S1). Typically, **1a** (100 μM) was mixed with 0.25 equiv of different photocatalysts in PBS/CH_3CN (8/2, v/v) and subjected to light irradiation for 30 min, followed by addition of probe-1 (200 μM) and incubation at 37 °C for another 6 h before measuring fluorescence. Results showed that green-light excited RB achieved the most significant emission enhancement (Figure 3, lower panel, peak at 530 nm), which is comparable to the emission intensity by incubating probe-1 with NHC-Au-Cl (Figure S1a). In the case of using the red-light absorbing MB as a photocatalyst, a slightly lower but still decent fluorescence intensity was observed (Figure 3, lower panel). Meanwhile, the transition-metal photocatalysts were unfavorable to this transformation.

With the preliminary results in hand, we then characterized the photoreactivity of **1a** with RB by HPLC analysis. After the mixture was irradiated for 30 min by 530 nm light in PBS/CH_3CN (8/2, v/v), the signal of **1a** (retention time = 9.9 min) totally disappeared, in association with a new peak (retention time = 6.5 min) which matched with that of NHC-Au-Cl dissolved in the same solvent (see Figure 4a and Figure S2). In the meantime, insoluble precipitate was found. Then, we performed the photoreaction in CH_3CN, and the reaction products became soluble after photoirradiation. HPLC analysis showed a major peak that is consistent with 1,4-diphenylbuta-1,3-diyne (dpby) in the LC chromatogram (Figure S3). This was confirmed by a ^1H NMR experiment, showing the ^1H signals of dpby at δ = 7.62−7.43 ppm (see Figure 4b and Figure S4). Similar results were obtained by using MB and 630 nm light irradiation conditions (Figure S5). Further HRMS analysis showed the existence of NHC-Au-DMSO (m/z = 371.0488), NHC-Au-CH_3CN (m/z = 334.0607) in different solutions (Figures S6a−S6c), likely resulting from the hydrolysis of the reaction products.[120−122] These results are consistent with the above fluorescence assays and collectively indicated that **1a** could be transformed into active NHC-Au-L

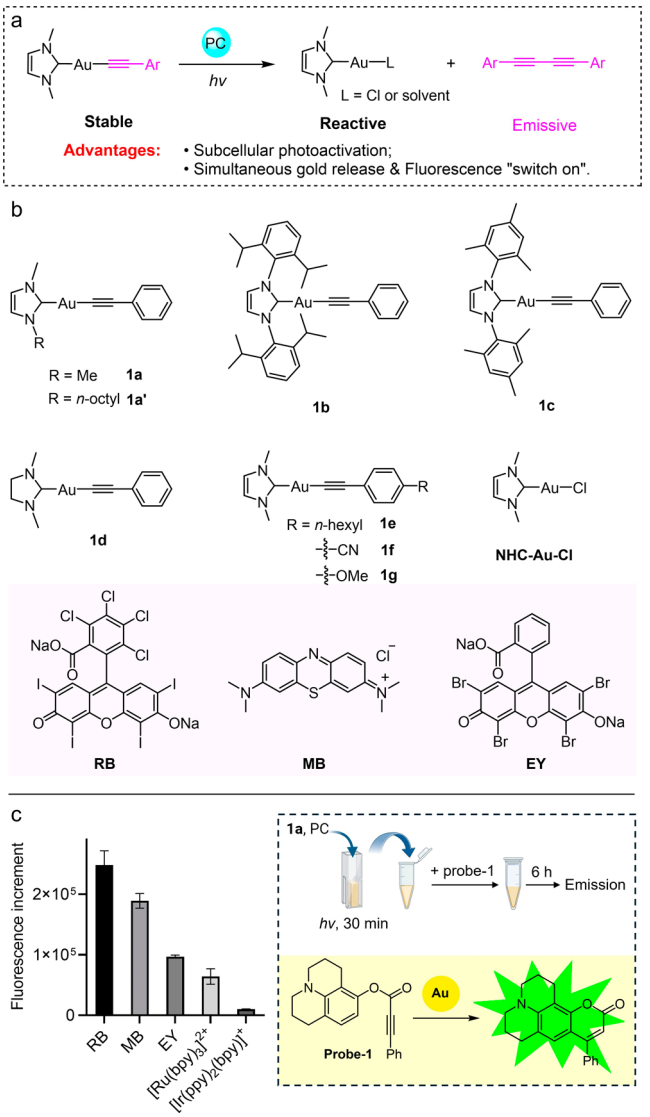

Figure 3. (a) Description of the photocatalytic transformation of stable **1a** into reactive NHC-Au-L (L = Cl or solvents) and its potential advantages. (b) Chemical structures of gold(I) complexes and photocatalysts. (c) Detection of the efficiency of generating reactive gold(I) by using probe-1. In this experiment, **1a** (100 μM) and PC (25 μM) in PBS/CH_3CN (8/2, v/v) were mixed and irradiated with light for 30 min. Then, probe-1 (200 μM) was added, and the mixture was further incubated in the dark for 6 h before the fluorescence intensity. The values of "Fluorescence increment" were calculated by the fluorescent intensity after incubating probe-1 with the photoactivated mixture subtracted by the same procedure but without light irradiation. The error bars indicate the standard deviations derived from three independent experiments. The inset shows the procedure and reaction mechanism by which probe-1 detects reactive gold(I) species. Created with permission from Biorender.com.

(L = Cl, solvent, or other weak donor ligands) by photocatalysts under buffer conditions (PBS/CH_3CN 8/2, v/v).

Afterward, we tried to understand the photoactivation mechanism. First, fluorescence quenching experiment showed that the emission intensity of RB was significantly suppressed by **1a** (Figure S7), suggestive of the possibility for SET to happen. When the free radical trap 2,2,6,6-tetramethylpiperidinyloxyl (TEMPO) was added, significantly diminished photo-

https://doi.org/10.1021/jacs.5c03186
J. Am. Chem. Soc. 2025, 147, 15719−15731

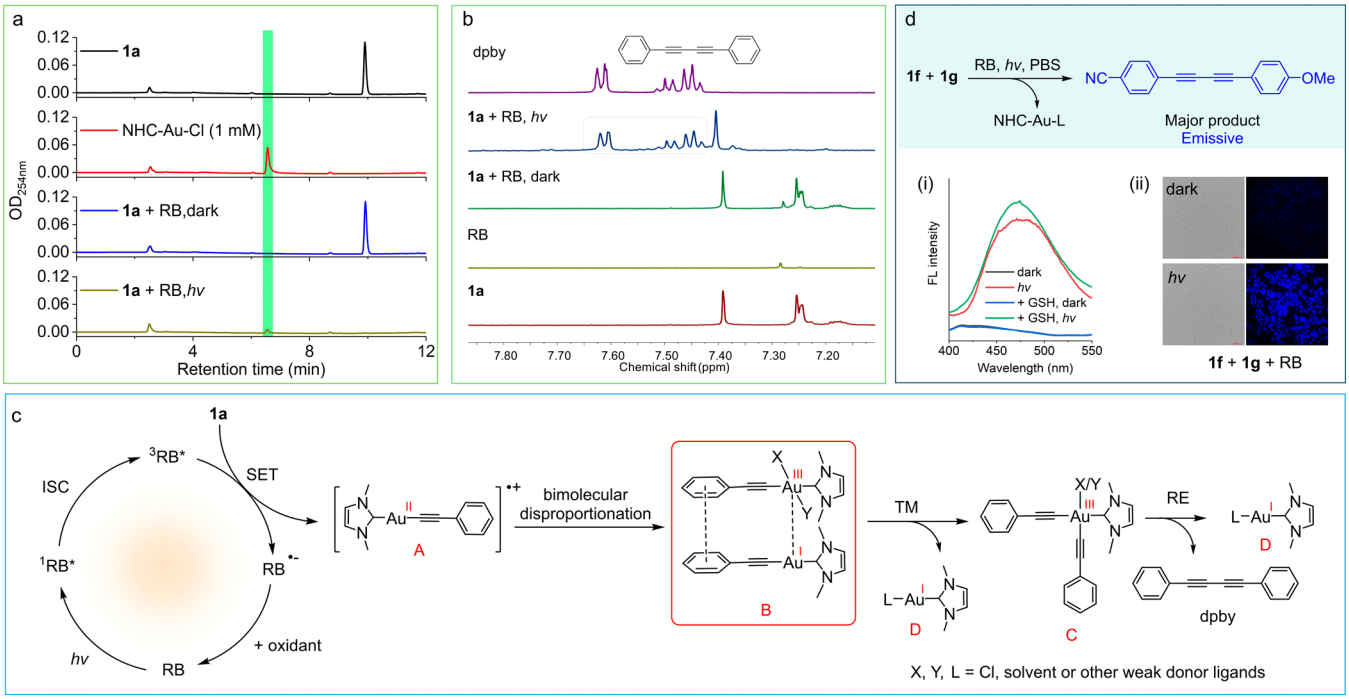

Figure 4. Photocatalytic reactivity and mechanism studies for photoactivation. (a) HPLC chromatograms for 1a (100 μM), NHC-Au-Cl (1 mM), the mixture of **1a** (100 μM) and RB (25 μM) in the dark, and the mixture of **1a** (100 μM) and RB (25 μM) after 530 nm light irradiation for 30 min in aqueous solution. (b) ^{1}H NMR analysis for the photoreaction of **1a** (1 mM) and RB (0.25 mM) after 530 nm light irradiation for 90 min in d_6-DMSO, showing formation of dpby. (c) The proposed photocatalytic mechanisms: **1a** is first oxidized by triplet excited state of RB (^{3}RB*), generating a gold(II) species that can undergo bimolecular disproportionation and transmetalation (TM), forming one molecule of NHC-Au-L and a gold(III) species carrying two phenylacetylene ligands; the subsequent reductive elimination (RE) yields an additional molecule of NHC-Au-L. (d) Photoreaction of **1f**, **1g**, and RB after 530 nm light irradiation generates the cross-coupling product diyne(CN-OMe) that is emissive. The emission intensity of **1f**, **1g**, and RB after 530 nm photoirradiation in PBS/CH_3CN (8/2, v/v) with or without GSH was shown (i), and the fluorescence microscopic images of A549 cells after photoirradiation of the cells treated by **1f**, **1g**, and RB were depicted (ii). Scale bar = 100 μM.

reactivity was found (Figure S3), indicative of involving radical species. Of note, when **1a** was replaced with **1b** or **1c** bearing two bulky N-substituents on NHC, no obvious conversion was found under the same irradiation conditions (Figures S8a and S8b). Instead, **1a′**, **1d** and **1e** containing less hindered N-substituents can undergo similar photochemical transformations (Figures S9a–S9c). Considering the phenomenon in which dpby was formed during photoactivation, it appears that there was a bimolecular process.

To demonstrate the existence of digold intermediate, we used two analogues **1f** and **1g**, which were added one-pot to the photoreaction mixture. After irradiating with 530 nm light for 30 min, HPLC analysis indicated the formation of the cross-coupling 4-((4-methoxyphenyl)buta-1,3-diyn-1-yl)-benzonitrile (diyne(CN-OMe)) as the major product (Figure S10), with the homocoupling 1,4-bis(4-methoxyphenyl)buta-1,3-diyne ($OMeyne_2$) as a minor one, which is fully supportive of the bimolecular process (formation of the byproduct $OMeyne_2$ but not $CNyne_2$ is possibly due to a lower reactivity of **1f** than **1g** that hinders the intermolecular recombination). In addition, the necessity of adding O_2 to this transformation was examined. When the reaction mixture was fully degassed by three freeze–pump–thaw cycles, no obvious reaction was found (Figure S11), suggesting that an oxidant is required for the reaction. Nevertheless, the photoreaction proceeded very well under hypoxia (1 vol % O_2) with similar efficiency to the aerobic conditions (Figure S12).

Based on these results, the following mechanism was proposed (Figure 4c). Complex **1a** is first oxidized by the photoexcited RB into a strongly reactive Au(II) radical **A** via SET, and then two molecules of Au(II) could recombine and proceed disproportionation,[123] forming a mixed-valent digold complex **B**.[124] This bimolecular intermediate could facilely undergoes ligand transfer to give one molecule of active Au(I) **D**, accompanied by the production of dialkynylgold(III) intermediate **C**, which could provide another molecule of **D**, together with the reductive elimination product dpby.[124,125] Consistent with this reductive-elimination mechanism, when **1h**, the gold(I) complex containing two *p*-fluorophenylacetylene ligands, was subjected to similar photoreaction conditions, the elimination product 1,4-bis(4-fluorophenyl)buta-1,3-diyne (Fdpby) was detected (Figure S13).

Photocatalysis Abrogates GSH Interference and Provides Robust Activation Efficiency in Cancer Cells. Based on the radical photoactivation mechanism, we next examined whether the photocatalytic approach could conquer the influence of physiological GSH for robust activation within cancer cells. In this regard, millimolar concentration of GSH was added to the mixture of **1a** and RB before photoirradiation, and the previously reported Pd(II)-mediated transmetalation reaction was examined for comparative study.[37] First, HPLC analysis showed that in the presence of 1 mM of GSH, almost full conversion (>95%) of **1a** could be found after photoirradiation for 30 min with RB; however, more than 55% of **1a** remained intact in the Pd(II)-mediated transmetalation. When 2 mM of GSH is present, over 85% conversion of **1a** was found after photoirradiation for 1 h with RB, but <10% of **1a** reacted in transmetalation condition

https://doi.org/10.1021/jacs.5c03186
J. Am. Chem. Soc. 2025, 147, 15719−15731

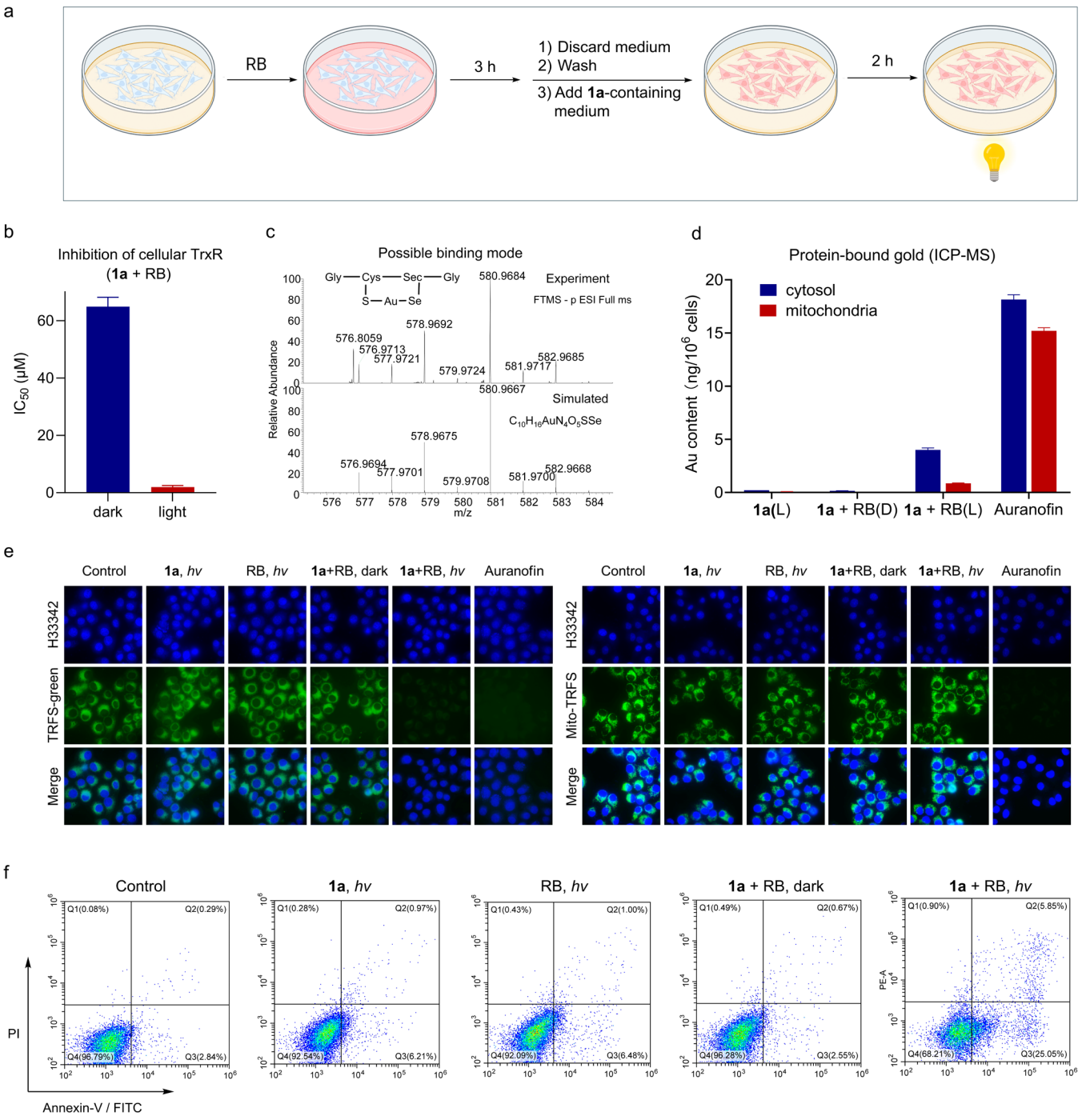

Figure 5. Selective inhibition of TrxR1 and induction of apoptosis in cancer cells. (a) Description of the general process for cell-based experiments which exclude the outside photoreactions.[126] In general, the cells were treated with PC for 3 h; then, the PC-containing medium was removed, and the cells were washed twice. Afterward, the medium containing **1a** was added and incubated for another 2 h before light irradiation for 10 min. Created with permission from Biorender.com. (b) Total cellular TrxR activity: A549 cells were treated with the "**1a** + RB" combo under dark or light conditions, and then the cells were lysed and measured using the DTNB/TrxR/NADPH assay (added with GR inhibitor). (c) HRMS spectrum for the mixture of GCUG peptide (100 μM) with photoactivated **1a** (100 μM) by RB (25 μM). Please refer to the full spectrum in Figure S20. (d) Protein-bound gold (covalently/coordinatively) after incubating A549 cells in the indicated treatment conditions, where the (subcellular) cell lysates were precipitated by acetone, washed, and the proteins were collected for ICP-MS analysis. (e) Fluorescence images of A549 cells after the treatments following the process shown in panel (a), and the cells were subsequently stained with Hoechst 33342 (H33342) and either TRFS-green or Mito-TRFS under various conditions. (f) Flow cytometry analysis for A549 cells following the treatment as shown in panel (a) and labeled with annexin V-FITC and PI under different conditions.

(Figures S14a and S14b). Then we used probe-1 to examine the catalytic activity of the activated gold species (Figures S15a and S15b). It was found that both transmetalation and photocatalysis could boost the catalytic activity of **1a** in the absence of GSH. However, when 0.5 mM GSH (5-fold to **1a**) was present, the activation efficiency of transmetalation was greatly attenuated, with only 14% fluorescence intensity, compared to GSH-free conditions. When the concentration

https://doi.org/10.1021/jacs.5c03186
J. Am. Chem. Soc. 2025, 147, 15719−15731

of GSH was increased to 1 mM, the capability of transmetalation for the activation of **1a** was completely abolished as depicted by negligible fluorescence enhancement. In contrast, under the same situation, the reaction efficiency via photocatalysis approach was not affected as indicative of similar level of fluorescence enhancement compared to GSH-free counterpart, and maintained 11-fold emission increase, even when 2 mM GSH was present.

Compound diyne (CN-OMe), produced from the photoreaction in the **1f** and **1g** mixture (Figure 4d), has typical D-π-A character and is highly emissive. Indeed, photoirradiation of the reaction mixture is accompanied by an ∼20-fold increase of emission intensity at 475 nm (Figure 4d(i). Of note, such a fluorescence switch on phenomenon could still be observed in the presence of GSH, and again HPLC analysis showed that the phototriggered cross-coupling proceeded equally well in the presence of GSH with no obviously compromised efficiency (Figure S16). With these results in hand, we then examined the phototriggered cross-coupling reaction in living cells by fluorescence microscopy. Human lung adenocarcinoma A549 cells were treated with **1f**, **1g**, and RB for 4 h, the culture solution was removed and changed with fresh medium, and then the cells were subjected to 530 nm light irradiation for 10 min. The cells were imaged after replacing the medium with PBS. As shown in Figure 4d(ii), the cells treated with **1f** and **1g** in the dark did not exhibit any notable blue fluorescence, yet the cells cotreated with **1f** and **1g** followed by light irradiation displayed bright blue fluorescence mainly in the cytoplasmic region of cancer cells, which is consistent with the results in aqueous solution, suggesting the efficient photocatalysis-enabled reductive elimination process in living cells. Furthermore, the photocatalytic reaction was found to be accompanied by release of active gold species as revealed from the strong red emission in living *E. coli* cells carrying a gold-specific biosensor GolS-mCherry (Figure S17),[127] and the released gold could exert catalytic functions inside living cells by using probe-1 (Figure S18).[128−133] Thus, these results demonstrated that the strong Au−C (acetylide) bond could be broken down via photocatalysis, leading to the release of active gold(I) species in living cells.

Subcellular Photocatalysis Results in Selective Inhibition of TrxR1 over TrxR2 in Cancer Cells. Given that RB can efficiently convert stable **1a** into active gold inside cancer cells, we tested the ability of the "**1a** + RB" combo to inhibit cellular TrxR,[8,9,12] following the treatment procedure as shown in Figure 5a.[134−136] Initially, the total TrxR activity of A549 cell lysates was assayed. Results illustrated in Figure 5b showed that while the "**1a** + RB" combo showed low TrxR inhibition in the dark with IC_{50} value of 64.9 ± 2.4 μM, it effectively inhibited TrxR with IC_{50} of 2.0 ± 0.4 μM after light irradiation, which is only slightly weaker than the potent TrxR inhibitor auranofin (IC_{50} = 0.67 ± 0.13 μM). In the control, the cells treated with RB only followed by light irradiation did not show noticeable inhibition (Figure S19). A possible binding mode with TrxR was examined by using the active site of TrxR Gly-Cys-Sec-Gly (GCUG) tetrapeptide. After incubating GCUG with the "**1a** + RB" combo under light irradiation, high-resolution mass spectrometry (HRMS) showed that the m/z (580.9684) and isotopic pattern matched well with a naked Au^+ simultaneously bound with the S and Se of GCUG peptide (see Figure 5c and Figure S20). Binding of active gold species (NHC-Au) toward the thiol-containing model protein BSA or HSA was also observed (Figures S21a and S21b). These results indicated that **1a** could be efficiently photoactivated by RB to release active gold(I) species that can potently inhibit TrxR through a tight binding mode.

As mentioned previously, the photosensitizers can easily escape from endosome/lysosome and accumulate in cytosol by low dose irradiation,[66,111−114] so we checked whether RB and MB can induce a selective activation and inhibition to TrxR1. First, the subcellular distribution of **1a** in A549 cells before activation were examined (Figure S22), showing a random distribution in cytosol and mitochondria. Then, A549 cells were treated with RB for 3 h, followed by medium removal and cell washing, and subsequently, **1a**-containing medium was added for another 2 h incubation before 530 nm light irradiation for 10 min (Figure 5a). After a further 2 h incubation, the subcellular components were harvested separately, and the protein-bound gold was detected by ICP-MS analysis on the precipitates after acetone precipitation. As the results show in Figure 5d, the gold contents (covalently/coordinatively bound) in the protein precipitates were increased significantly compared to the dark control group. Especially, the cytosolic protein-bound gold was enriched to 4.0 ng in cytosol per 10^6 cells, accounting for 83% of the whole cellular protein-bound gold (4.8 ng per 10^6 cells), suggestive of a selective activation within cytosol. In contrast, cancer cells treated with auranofin showed 46% of protein-bound gold in mitochondria. Then, we employed TRFS-green, a TrxR-responsive fluorescence off-on probe that is mainly localized in cytosol,[137] and Mito-TRFS, a selective mitochondrial TrxR2 fluorescent probe (note: gold did not have direct interference on the unactivated and activated probes, Figures S23a and S23b).[137] As depicted in Figure 5e, while the control cells treated by **1a** with light, RB with light, or "**1a** + RB" in the dark showed bright green emission, cancer cells treated by "**1a** + RB" after light irradiation showed significantly diminished emission intensity in the TRFS-green staining group but not in the Mito-TRFS condition, suggestive of a selective TrxR1 inhibition. For comparison, A549 cells treated by auranofin, a pan TrxR inhibitor, significantly decreased the emission intensity in both TRFS-green and Mito-TRFS conditions. We have further isolated the treated cells by subcellular fractionation and tested the TrxR activity by colorimetric assay, which yielded consistent results (see Figures S24a and S24b). When red-light absorbing MB was used as a photocatalyst, similar results were detected (see Figures S25 and S26). For comparison, direct use of the reactive NHC-containing gold(I) complexes did not show selectivity (Figure S27). Thus, the photocatalytic activation can indeed offer an advantage to induce subcellular activation for targeted inhibition of TrxR1. It should be noted that due to the capability of serum albumin in the medium to bind active gold species outside the cells (Figure S28), no obvious difference was found if **1a** and RB were added one-pot without the washing step for the cell-based experiments (Figure S29).

Subcellular Photocatalysis Results in Potent Cytotoxicity to Cancer Cells. Next, we examined the possible cellular responses after TrxR inhibition (following a similar cell treatment procedure shown in Figure 5a). First, we conducted DCFH-DA staining to estimate the cellular ROS level. When A549 cells were treated by "**1a** + RB" followed by light irradiation, strong green fluorescence was observed intracellularly whereas no obvious emission was found in the absence of either photocatalyst, **1a** or light irradiation (Figure S30). Afterward, the mitochondrial membrane potential was

https://doi.org/10.1021/jacs.5c03186
J. Am. Chem. Soc. 2025, 147, 15719−15731

examined by JC-1 staining. Results showed a strong green emission in A549 cells treated by the photoactivated gold with little red fluorescence, but the control groups only gave red emission without green color (Figure S31), indicative of mitochondrial depolarization that may be associated with apoptosis.[138] Then, the possibility of the photoactivated gold for induction of apoptosis was carried out by using annexin V-FITC and PI co-staining. Flow cytometry analysis (Figure 5f) showed 31.8% of apoptotic cells (including both early and late stage) in the "**1a** + RB" under the light group. For comparison, less than 10% of apoptotic cells were found in the groups without **1a**, RB, or light irradiation.

Subsequently, the cytotoxicity of the gold(I) complexes in combination with RB against lung carcinoma A549 cells was investigated by MTT assays. The results were summarized in Table 1 and Table S2. All complexes are less-toxic in dark conditions with IC_{50} > 60 μM after 48 h of incubation. Instead, the addition of RB followed by 530 nm light irradiation significantly increased the cytotoxicity of **1a** with IC_{50} values of 7.4 μM in normoxia and 8.2 μM in acute hypoxia (O_2 < 1%). The reductive elimination product 1,4-diphenylbuta-1,3-diyne (dpby) did not show noticeable TrxR inhibition or cytotoxicity at 100 μM. Complex **1e** with a long alkyl chain displayed slightly better combinatorial effect with RB compared to **1a**, probably due to its higher lipophilicity that is beneficial to cellular uptake. It is worth noting that **1b** showed no apparent therapeutic effects under the same conditions, which was consistent with the above-mentioned mechanism studies. Similar combined therapeutic effect of **1a** and RB was found in human melanoma A375 and cervical cancer HeLa cells (Table 1). Importantly, in view of the fact that MB is also a good photocatalyst for this transformation and displays a longer absorption in the red region, we tested whether MB could activate the cytotoxicity of the gold(I) complexes in cancer cells. As shown in Table S3, both **1a** and **1e** can be activated by MB under 630 nm light irradiation under acute hypoxic conditions (O_2 < 1%), with a 6- to 14-fold increase in cytotoxicity. We further checked whether the specific inhibition of cytosolic TrxR1 over mitochondrial TrxR2 could lead to selective cytotoxicity against cancer cells while sparing normal ones. To this end, the cytotoxicity of the "**1a** + RB" combo toward normal cells, including human umbilical vein endothelial cell line HUVEC and human colon cell line NCM460, was examined for comparative study. Results shown in Table 1 indicate that the "**1a** + RB" combo was generally less cytotoxic toward normal cell lines (IC_{50} of 15.3−16.6 μM) than that toward cancer cells such as A549, A375, and HeLa, with IC_{50} of 4.7−8.5 μM, i.e., up to 3.6-fold selectivity. Similar cytotoxicity was found following the procedure depicted in Figure 5a after a total of 48 h of incubation (Table S4), whereas the pan TrxR inhibitor, auranofin, failed to display selectivity under the same conditions.

Table 1. Cytotoxicity (μM)[a] of the "1a + RB" Combo in Dark (D) or Light (L)[b] Conditions toward Different Cancer and Normal Cells

	Cytotoxicity (μM)				
	A549	A375	HeLa	HUVEC	NCM460
Combo(D)	74.8 ± 9.7	61.9 ± 8.0	65.2 ± 3.8	70.0 ± 7.4	85.4 ± 4.5
Combo(L)	7.4 ± 2.2	4.7 ± 1.9	8.5 ± 1.1	15.3 ± 3.1	16.6 ± 1.9
PI[c]	10.1	13.2	7.7	4.6	5.1
AuRF[d]	4.4 ± 0.5	1.1 ± 0.1	2.3 ± 0.5	3.6 ± 0.1	2.6 ± 0.5

[a]Total incubation of 48 h. [b]Cells in RB (5 μM) alone under light irradiation maintain at least >80% cell viability. [c]PI = photoindex. [d]Auranofin (AuRF) was also tested for comparison.

Subcellular Photocatalysis Leads to Robust Anticancer Activities In Vivo. Afterward, we investigated if photocatalytic activation works under in vivo conditions by using the red-light-absorbing MB as photocatalyst. Initially, wild-type zebrafish was used to examine the catalytic activity. The zebrafish was treated with **1a** and MB, together with probe-1 as a reporter; bright coumarin green emission was observed after 630 nm light irradiation for 10 min (Figure S32), suggestive of efficient generation of active gold species. Considering that active gold(I) is antiangiogenic with capability to inhibit forming blood vessels,[34] we used a transgenic zebrafish line (GFP-Lc3) expressing green fluorescent protein in vasculatures[139] to examine whether the active Au(I) species generated by photocatalytic activation may elicit antiangiogenesis activity in vivo. The embryos were treated with the "**1a** (10 μM) + MB (2.5 μM)" combo, followed by 630 nm light irradiation for 10 min. Three days later, the fluorescence images were captured by inverted fluorescence microscope. As the results show in Figure S33a, the "**1a** + MB" combo under red-light treatment potently suppressed angiogenesis particularly in the intersegmental vessels (ISV) and dorsal longitudinal anastomotic vessels (DLAV). In the control, negligible change was observed in the groups treated with **1a** only, MB only, or "**1a** + MB" in the dark. Besides, similar results could be found when RB was used as a photocatalyst under 530 nm irradiation (Figure S33b). The antitumor activities were also tested in the zebrafish tumor models. The HCT116 cells stably expressing EGFP were microinjected into the yolk sac of new-born wild-type zebrafish. Two days later, the zebrafish bearing HCT116/GFP tumor xenografts was treated with "**1a** + MB" combo along with 630 nm light irradiation for 10 min. One day after treatment, the fluorescence images were collected. As the results depicted in Figure 6a, the "**1a** + MB" combo with red light irradiation significantly suppressed tumor growth as indicated by reduced green emission by 60% (p < 0.05) in comparison with solvent control group. It should be noted that MB alone under light irradiation did not show significant inhibition of the fluorescence intensity under similar conditions.

We further examined the in vivo antitumor activity of the "**1a** + MB" combo using mice bearing A549 tumor xenograft (Figure 6b). In general, A549 cells were inoculated (s.c.) in the right flank of mice. Five days later, the tumor-bearing mice were treated with the "**1a** + MB" once every two or 3 days for a total five times treatment, and the tumors were irradiated with 635 nm light for 4 h each post-treatment (Figure 6b(i). After 22 days, the "**1a** + MB" group, after 635 nm irradiation, strongly suppressed tumor growth by 83% compared to the solvent control (Figure 6b(ii−iv)). In the case of MB under light irradiation, only ∼30% tumor inhibition was found, without statistical significance. The treatment did not cause mouse death or mouse body weight loss.

CONCLUSION

In summary, a subcellular photocatalytic strategy was developed to controllably activate organogold(I) prodrugs

https://doi.org/10.1021/jacs.5c03186
J. Am. Chem. Soc. 2025, 147, 15719−15731

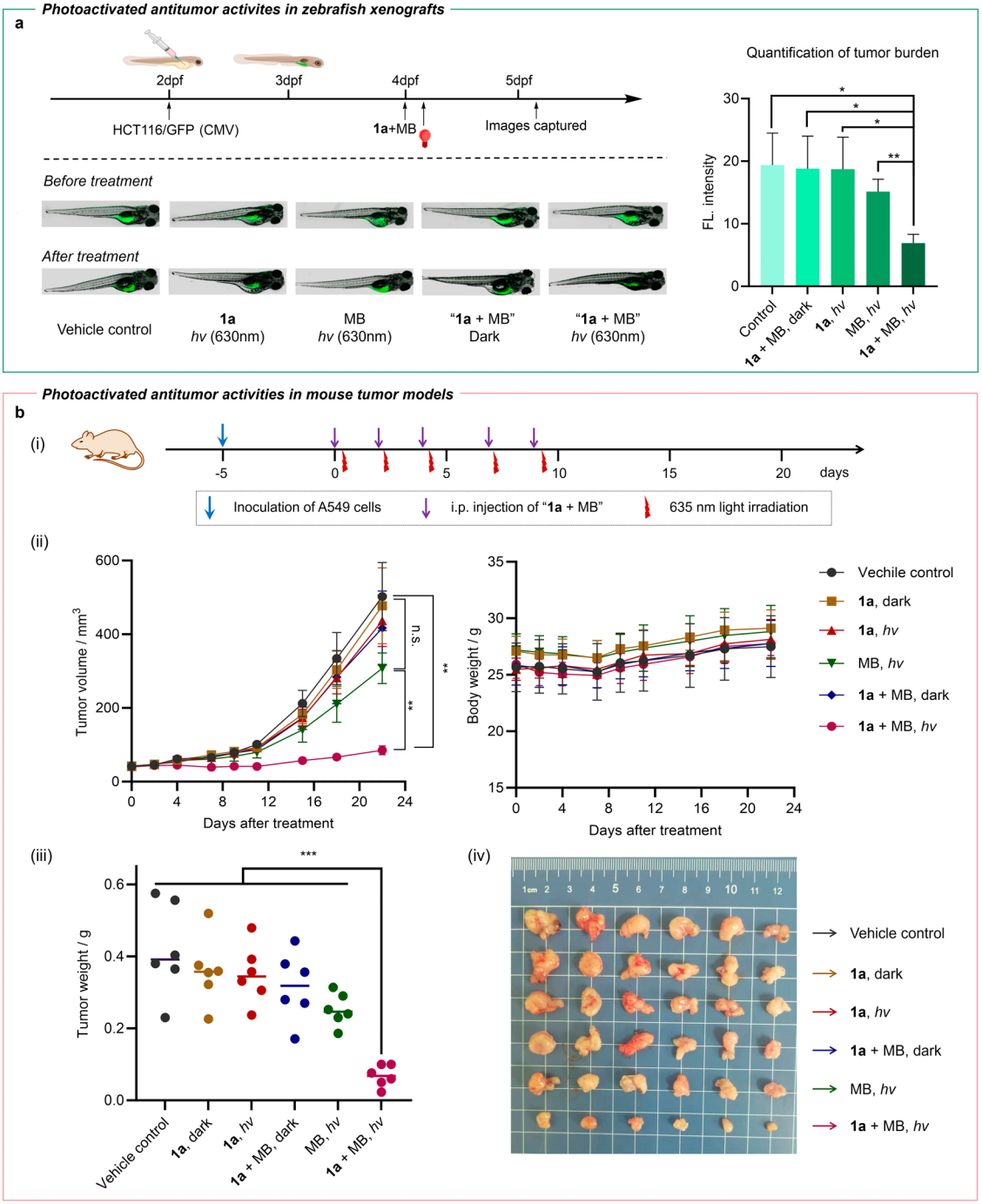

Figure 6. Red light-activated antitumor activity in vivo. (a) Inhibition of tumor growth in zebrafish bearing HCT116/GFP xenografts, where the green fluorescence in zebrafish indicates tumor burden. The cartoon images of zebrafish were created with permission from Biorender.com. (b) Description of the timeline for the mouse experiment (i) during which A549 cells were inoculated in the right flank of mice by subcutaneous injection 5 days before drug administration. The tumor-bearing mice (n = 6 for each group) were treated by the "**1a** (3 mg/kg) + MB (2 mg/kg)" combo on day 0, 2, 4, 7, 9 and were irradiated with 635 nm LED light for 4 h each post-injection. Tumor volume (ii, left) and body weight (ii, right), tumor weight (iii) and tumor images (iv) were shown. [Legend: (*) $p < 0.05$, (**) $p < 0.01$, (***) $p < 0.001$.]

within cytosol for targeted inhibition of tumor-associated TrxR1. The organogold(I) complexes are stable under physiological conditions, effectively preventing off-target interactions, particularly with extracellular serum albumin. However, after a short green/red light irradiation time, it can be transformed into active Au(I) species with almost quantitative yield at the target site. Mechanistic studies show that a photoinduced radical-bimolecular reductive process was involved, which can greatly decrease glutathione interference in solution and in living cells. Such a character was harnessed and demonstrated useful for controlled activation in the cytosol over mitochondria due to the capability of photocatalysts that can escape from endosomal trapping and accumulate in cytosol. This enables selective photocatalytic conversion of organogold(I) complexes into active NHC-Au-Cl within the cytosol, leading to targeted inhibition of TrxR1 rather than

https://doi.org/10.1021/jacs.5c03186
J. Am. Chem. Soc. 2025, 147, 15719−15731

TrxR2, along with potent cytotoxicity to cancer cells. Of note, the photocatalytic prodrug system displays a significantly higher selectivity than auranofin—a pan TrxR inhibitor unable to differentiate between TrxR1 and TrxR2, and shows robust antitumor activity in vivo in tumor xenografts. This platform may allow additional strategies such as conjugating tumor targeting peptides or using drug delivery system to further improve the selectivity toward cancer cells.[140,141] In view of the capability of photocatalysis in the activation of different prodrugs and the ease with which the system can be built, this subcellular photocatalytic activation strategy holds the potential to be extended to differentiate and target other enzyme isoforms with distinct organelle specificity and functions, which, we believe, may open a new avenue for precision therapies.

■ ASSOCIATED CONTENT

Supporting Information

The Supporting Information is available free of charge at https://pubs.acs.org/doi/10.1021/jacs.5c03186.

Experimental procedures for the chemical synthesis, characterization, photoreactions, cell-based biological experiments, and in vivo antitumor experiments (PDF)

■ AUTHOR INFORMATION

Corresponding Authors

Xiaolin Xiong − *State Key Laboratory of Anti-Infective Drug Discovery and Development, Guangdong Key Laboratory of Chiral Molecule and Drug Discovery, School of Pharmaceutical Sciences, Sun Yat-Sen University, Guangzhou 510006, P. R. China*; Email: xiongxlin@mail.sysu.edu.cn

Taotao Zou − *State Key Laboratory of Anti-Infective Drug Discovery and Development, Guangdong Key Laboratory of Chiral Molecule and Drug Discovery, School of Pharmaceutical Sciences, Sun Yat-Sen University, Guangzhou 510006, P. R. China*; orcid.org/0000-0001-9129-4398; Email: zoutt3@mail.sysu.edu.cn

Authors

Moyi Liu − *State Key Laboratory of Anti-Infective Drug Discovery and Development, Guangdong Key Laboratory of Chiral Molecule and Drug Discovery, School of Pharmaceutical Sciences, Sun Yat-Sen University, Guangzhou 510006, P. R. China*

Haitao Liu − *State Key Laboratory of Anti-Infective Drug Discovery and Development, Guangdong Key Laboratory of Chiral Molecule and Drug Discovery, School of Pharmaceutical Sciences, Sun Yat-Sen University, Guangzhou 510006, P. R. China*

Yan Yang − *State Key Laboratory of Anti-Infective Drug Discovery and Development, Guangdong Key Laboratory of Chiral Molecule and Drug Discovery, School of Pharmaceutical Sciences, Sun Yat-Sen University, Guangzhou 510006, P. R. China*

Complete contact information is available at: https://pubs.acs.org/10.1021/jacs.5c03186

Notes

The authors declare no competing financial interest.

■ ACKNOWLEDGMENTS

This work was finically supported by National Natural Science Foundation of China (Nos. 22377154, 22122706), Major Program of Guangzhou National Laboratory (No. GZNL2023A02012), Guangdong Basic and Applied Basic Research Foundation (Nos. 2024B1515040028, 2024A151501072), Guangdong Science and Technology Department (No. 2019QN01C125), Guangzhou Science and Technology Projects (No. 2024A04J6478), and Guangdong Provincial Key Laboratory of Construction Foundation (No. 2023B1212060022).

■ REFERENCES

(1) D'Autréaux, B.; Toledano, M. B. ROS as signalling molecules: mechanisms that generate specificity in ROS homeostasis. *Nat. Rev. Mol. Cell Biol.* **2007**, *8*, 813.

(2) Dickinson, B. C.; Chang, C. J. Chemistry and biology of reactive oxygen species in signaling or stress responses. *Nat. Chem. Biol.* **2011**, *7*, 504.

(3) Lennicke, C.; Cochemé, H. M. Redox metabolism: ROS as specific molecular regulators of cell signaling and function. *Mol. Cell* **2021**, *81*, 3691.

(4) Cheng, Q.; Sandalova, T.; Lindqvist, Y.; Arnér, E. S. J. Crystal Structure and Catalysis of the Selenoprotein Thioredoxin Reductase 1. *J. Biol. Chem.* **2009**, *284*, 3998.

(5) Bjørklund, G.; Zou, L.; Wang, J.; Chasapis, C. T.; Peana, M. Thioredoxin reductase as a pharmacological target. *Pharmacol. Res.* **2021**, *174*, 105854.

(6) Sadler, P. J.; Sue, R. E. The Chemistry of Gold Drugs. *Met.-Based Drugs* **1994**, *1*, 107.

(7) Shaw, C. F. Gold-Based Therapeutic Agents. *Chem. Rev.* **1999**, *99*, 2589.

(8) Ott, I. On the medicinal chemistry of gold complexes as anticancer drugs. *Coord. Chem. Rev.* **2009**, *253*, 1670.

(9) Nobili, S.; Mini, E.; Landini, I.; Gabbiani, C.; Casini, A.; Messori, L. Gold compounds as anticancer agents: chemistry, cellular pharmacology, and preclinical studies. *Med. Res. Rev.* **2010**, *30*, 550.

(10) Berners-Price, S. J.; Filipovska, A. Gold compounds as therapeutic agents for human diseases. *Metallomics* **2011**, *3*, 863.

(11) Muhammad, N.; Guo, Z. Metal-based anticancer chemotherapeutic agents. *Curr. Opin. Chem. Biol.* **2014**, *19*, 144.

(12) Zou, T.; Lum, C. T.; Lok, C.-N.; Zhang, J.-J.; Che, C.-M. Chemical biology of anticancer gold(III) and gold(I) complexes. *Chem. Soc. Rev.* **2015**, *44*, 8786.

(13) Mora, M.; Gimeno, M. C.; Visbal, R. Recent advances in gold−NHC complexes with biological properties. *Chem. Soc. Rev.* **2019**, *48*, 447.

(14) Thomas, S. R.; Casini, A. Gold compounds for catalysis and metal-mediated transformations in biological systems. *Curr. Opin. Chem. Biol.* **2020**, *55*, 103.

(15) Gamberi, T.; Pratesi, A.; Messori, L.; Massai, L. Proteomics as a tool to disclose the cellular and molecular mechanisms of selected anticancer gold compounds. *Coord. Chem. Rev.* **2021**, *438*, 213905.

(16) Lu, Y.; Ma, X.; Chang, X.; Liang, Z.; Lv, L.; Shan, M.; Lu, Q.; Wen, Z.; Gust, R.; Liu, W. Recent development of gold(I) and gold(III) complexes as therapeutic agents for cancer diseases. *Chem. Soc. Rev.* **2022**, *51*, 5518.

(17) Moreno-Alcántar, G.; Picchetti, P.; Casini, A. Gold Complexes in Anticancer Therapy: From New Design Principles to Particle-Based Delivery Systems. *Angew. Chem., Int. Ed.* **2023**, *62*, No. e202218000.

(18) Mertens, R. T.; Gukathasan, S.; Arojojoye, A. S.; Olelewe, C.; Awuah, S. G. Next Generation Gold Drugs and Probes: Chemistry and Biomedical Applications. *Chem. Rev.* **2023**, *123*, 6612.

(19) Barnard, P. J.; Wedlock, L. E.; Baker, M. V.; Berners-Price, S. J.; Joyce, D. A.; Skelton, B. W.; Steer, J. H. Luminescence Studies of the Intracellular Distribution of a Dinuclear Gold(I) N-Heterocyclic Carbene Complex. *Angew. Chem., Int. Ed.* **2006**, *45*, 5966.

(20) Ray, S.; Mohan, R.; Singh, J. K.; Samantaray, M. K.; Shaikh, M. M.; Panda, D.; Ghosh, P. Anticancer and Antimicrobial Metallopharmaceutical Agents Based on Palladium, Gold, and Silver N-Heterocyclic Carbene Complexes. *J. Am. Chem. Soc.* **2007**, *129*, 15042.
(21) Hickey, J. L.; Ruhayel, R. A.; Barnard, P. J.; Baker, M. V.; Berners-Price, S. J.; Filipovska, A. Mitochondria-Targeted Chemotherapeutics: The Rational Design of Gold(I) N-Heterocyclic Carbene Complexes That Are Selectively Toxic to Cancer Cells and Target Protein Selenols in Preference to Thiols. *J. Am. Chem. Soc.* **2008**, *130*, 12570.
(22) Cisnetti, F.; Gautier, A. Metal/N-Heterocyclic Carbene Complexes: Opportunities for the Development of Anticancer Metallodrugs. *Angew. Chem., Int. Ed.* **2013**, *52*, 11976.
(23) Liu, W.; Gust, R. Update on metal N-heterocyclic carbene complexes as potential anti-tumor metallodrugs. *Coord. Chem. Rev.* **2016**, *329*, 191.
(24) Niu, W.; Chen, X.; Tan, W.; Veige, A. S. N-Heterocyclic Carbene-Gold(I) Complexes Conjugated to a Leukemia-Specific DNA Aptamer for Targeted Drug Delivery. *Angew. Chem., Int. Ed.* **2016**, *55*, 8889.
(25) Bazzicalupi, C.; Ferraroni, M.; Papi, F.; Massai, L.; Bertrand, B.; Messori, L.; Gratteri, P.; Casini, A. Determinants for Tight and Selective Binding of a Medicinal Dicarbene Gold(I) Complex to a Telomeric DNA G-Quadruplex: a Joint ESI MS and XRD Investigation. *Angew. Chem., Int. Ed.* **2016**, *55*, 4256.
(26) Fernández-Gallardo, J.; Elie, B. T.; Sanaú, M.; Contel, M. Versatile synthesis of cationic N-heterocyclic carbene-gold(I) complexes containing a second ancillary ligand. Design of heterobimetallic ruthenium-gold anticancer agents. *Chem. Commun.* **2016**, *52*, 3155.
(27) Wragg, D.; de Almeida, A.; Bonsignore, R.; Kühn, F. E.; Leoni, S.; Casini, A. On the Mechanism of Gold/NHC Compounds Binding to DNA G-Quadruplexes: Combined Metadynamics and Biophysical Methods. *Angew. Chem., Int. Ed.* **2018**, *57*, 14524.
(28) Zhang, C.; Fortin, P.-Y.; Barnoin, G.; Qin, X.; Wang, X.; Fernandez Alvarez, A.; Bijani, C.; Maddelein, M.-L.; Hemmert, C.; Cuvillier, O.; Gornitzka, H. An Artemisinin-Derivative-(NHC)Gold-(I) Hybrid with Enhanced Cytotoxicity through Inhibition of NRF2 Transcriptional Activity. *Angew. Chem., Int. Ed.* **2020**, *59*, 12062.
(29) Guarra, F.; Terenzi, A.; Pirker, C.; Passannante, R.; Baier, D.; Zangrando, E.; Gómez-Vallejo, V.; Biver, T.; Gabbiani, C.; Berger, W.; Llop, J.; Salassa, L. ^{124}I Radiolabeling of a AuIII-NHC Complex for In Vivo Biodistribution Studies. *Angew. Chem., Int. Ed.* **2020**, *59*, 17130.
(30) Sen, S.; Hufnagel, S.; Maier, E. Y.; Aguilar, I.; Selvakumar, J.; DeVore, J. E.; Lynch, V. M.; Arumugam, K.; Cui, Z.; Sessler, J. L.; Arambula, J. F. Rationally Designed Redox-Active Au(I) N-Heterocyclic Carbene: An Immunogenic Cell Death Inducer. *J. Am. Chem. Soc.* **2020**, *142*, 20536.
(31) Mule, R. D.; Kumar, A.; Sancheti, S. P.; Senthilkumar, B.; Kumar, H.; Patil, N. T. BQ-AurIPr: a redox-active anticancer Au(I) complex that induces immunogenic cell death. *Chem. Sci.* **2022**, *13*, 10779.
(32) Marciano, Y.; del Solar, V.; Nayeem, N.; Dave, D.; Son, J.; Contel, M.; Ulijn, R. V. Encapsulation of Gold-Based Anticancer Agents in Protease-Degradable Peptide Nanofilaments Enhances Their Potency. *J. Am. Chem. Soc.* **2023**, *145*, 234.
(33) Carlos Lima, J.; Rodríguez, L. Applications of gold(I) alkynyl systems: a growing field to explore. *Chem. Soc. Rev.* **2011**, *40*, 5442.
(34) Meyer, A.; Bagowski, C. P.; Kokoschka, M.; Stefanopoulou, M.; Alborzinia, H.; Can, S.; Vlecken, D. H.; Sheldrick, W. S.; Wölfl, S.; Ott, I. On the Biological Properties of Alkynyl Phosphine Gold(I) Complexes. *Angew. Chem., Int. Ed.* **2012**, *51*, 8895.
(35) Fernández-Moreira, V.; Marzo, I.; Gimeno, M. C. Luminescent Re(I) and Re(I)/Au(I) complexes as cooperative partners in cell imaging and cancer therapy. *Chem. Sci.* **2014**, *5*, 4434.
(36) Zhang, J.-J.; Abu el Maaty, M. A.; Hoffmeister, H.; Schmidt, C.; Muenzner, J. K.; Schobert, R.; Wölfl, S.; Ott, I. A Multitarget Gold(I) Complex Induces Cytotoxicity Related to Aneuploidy in HCT-116 Colorectal Carcinoma Cells. *Angew. Chem., Int. Ed.* **2020**, *59*, 16795.
(37) Long, Y.; Cao, B.; Xiong, X.; Chan, A. S. C.; Sun, R. W.-Y.; Zou, T. Bioorthogonal Activation of Dual Catalytic and Anti-Cancer Activities of Organogold(I) Complexes in Living Systems. *Angew. Chem., Int. Ed.* **2021**, *60*, 4133.
(38) Berners-Price, S. J.; Mirabelli, C. K.; Johnson, R. K.; Mattern, M. R.; McCabe, F. L.; Faucette, L. F.; Sung, C.-M.; Mong, S.-M.; Sadler, P. J.; Crooke, S. T. In Vivo Antitumor Activity and in Vitro Cytotoxic Properties of Bis[1,2-bis(diphenylphosphino)ethane]gold-(I) Chloride. *Cancer Res.* **1986**, *46*, 5486−5493.
(39) Elie, B. T.; Hubbard, K.; Layek, B.; Yang, W. S.; Prabha, S.; Ramos, J. W.; Contel, M. Auranofin-Based Analogues Are Effective Against Clear Cell Renal Carcinoma In Vivo and Display No Significant Systemic Toxicity. *ACS Pharmacol. Transl. Sci.* **2020**, *3*, 644.
(40) Yang, Z.; Huang, S.; Liu, Y.; Chang, X.; Liang, Y.; Li, X.; Xu, Z.; Wang, S.; Lu, Y.; Liu, Y.; Liu, W. Biotin-Targeted Au(I) Radiosensitizer for Cancer Synergistic Therapy by Intervening with Redox Homeostasis and Inducing Ferroptosis. *J. Med. Chem.* **2022**, *65*, 8401.
(41) Abogosh, A. K.; Alghanem, M. K.; Ahmad, S.; Al-Asmari, A.; As Sobeai, H. M.; Sulaiman, A. A. A.; Fettouhi, M.; Popoola, S. A.; Alhoshani, A.; Isab, A. A. A novel cyclic dinuclear gold(I) complex induces anticancer activity via an oxidative stress-mediated intrinsic apoptotic pathway in MDA-MB-231 cancer cells. *Dalton Trans.* **2022**, *51*, 2760.
(42) Sulaiman, A. A. A.; Casagrande, N.; Borghese, C.; Corona, G.; Isab, A. A.; Ahmad, S.; Aldinucci, D.; Altaf, M. Design, Synthesis, and Preclinical Activity in Ovarian Cancer Models of New Phosphanegold(I)-N-heterocyclic Carbene Complexes. *J. Med. Chem.* **2022**, *65*, 14424.
(43) Milacic, V.; Chen, D.; Ronconi, L.; Landis-Piwowar, K. R.; Fregona, D.; Dou, Q. P. A Novel Anticancer Gold(III) Dithiocarbamate Compound Inhibits the Activity of a Purified 20S Proteasome and 26S Proteasome in Human Breast Cancer Cell Cultures and Xenografts. *Cancer Res.* **2006**, *66*, 10478.
(44) Marzano, C.; Ronconi, L.; Chiara, F.; Giron, M. C.; Faustinelli, I.; Cristofori, P.; Trevisan, A.; Fregona, D. Gold(III)-dithiocarbamato anticancer agents: Activity, toxicology and histopathological studies in rodents. *Int. J. Cancer* **2011**, *129*, 487.
(45) Williams, M. R. M.; Bertrand, B.; Hughes, D. L.; Waller, Z. A. E.; Schmidt, C.; Ott, I.; O'Connell, M.; Searcey, M.; Bochmann, M. Cyclometallated Au(III) dithiocarbamate complexes: synthesis, anticancer evaluation and mechanistic studies. *Metallomics* **2018**, *10*, 1655.
(46) Le, H. V.; Babak, M. V.; Ehsan, M. A.; Altaf, M.; Reichert, L.; Gushchin, A. L.; Ang, W. H.; Isab, A. A. Highly cytotoxic gold(I)-phosphane dithiocarbamate complexes trigger an ER stress-dependent immune response in ovarian cancer cells. *Dalton Trans.* **2020**, *49*, 7355.
(47) Kolundžić, F.; Murali, A.; Pérez-Galán, P.; Bauer, J. O.; Strohmann, C.; Kumar, K.; Waldmann, H. A Cyclization-Rearrangement Cascade for the Synthesis of Structurally Complex Chiral Gold(I)−Aminocarbene Complexes. *Angew. Chem., Int. Ed.* **2014**, *53*, 8122.
(48) Fernández-Gallardo, J.; Elie, B. T.; Sadhukha, T.; Prabha, S.; Sanaú, M.; Rotenberg, S. A.; Ramos, J. W.; Contel, M. Heterometallic titanium-gold complexes inhibit renal cancer cells in vitro and in vivo. *Chem. Sci.* **2015**, *6*, 5269.
(49) Wirmer-Bartoschek, J.; Bendel, L. E.; Jonker, H. R. A.; Grün, J. T.; Papi, F.; Bazzicalupi, C.; Messori, L.; Gratteri, P.; Schwalbe, H. Solution NMR Structure of a Ligand/Hybrid-2-G-Quadruplex Complex Reveals Rearrangements that Affect Ligand Binding. *Angew. Chem., Int. Ed.* **2017**, *56*, 7102.
(50) Boscutti, G.; Nardon, C.; Marchiò, L.; Crisma, M.; Biondi, B.; Dalzoppo, D.; Dalla Via, L.; Formaggio, F.; Casini, A.; Fregona, D. Anticancer Gold(III) Peptidomimetics: From Synthesis to in vitro and ex vivo Biological Evaluations. *ChemMedChem.* **2018**, *13*, 1131.

(51) Fares, M.; Wu, X.; Ramesh, D.; Lewis, W.; Keller, P. A.; Howe, E. N. W.; Pérez-Tomás, R.; Gale, P. A. Stimuli-Responsive Cycloaurated ″OFF-ON″ Switchable Anion Transporters. *Angew. Chem., Int. Ed.* **2020**, *59*, 17614.
(52) Tong, K.-C.; Lok, C.-N.; Wan, P.-K.; Hu, D.; Fung, Y. M. E.; Chang, X.-Y.; Huang, S.; Jiang, H.; Che, C.-M. An anticancer gold(III)-activated porphyrin scaffold that covalently modifies protein cysteine thiols. *P. Natl. Acad. Sci. USA* **2020**, *117*, 1321.
(53) Babak, M. V.; Chong, K. R.; Rapta, P.; Zannikou, M.; Tang, H. M.; Reichert, L.; Chang, M. R.; Kushnarev, V.; Heffeter, P.; Meier-Menches, S. M.; Lim, Z. C.; Yap, J. Y.; Casini, A.; Balyasnikova, I. V.; Ang, W. H. Interfering with Metabolic Profile of Triple-Negative Breast Cancers Using Rationally Designed Metformin Prodrugs. *Angew. Chem., Int. Ed.* **2021**, *60*, 13405.
(54) Johnson, A.; Olelewe, C.; Kim, J. H.; Northcote-Smith, J.; Mertens, R. T.; Passeri, G.; Singh, K.; Awuah, S. G.; Suntharalingam, K. The anti-breast cancer stem cell properties of gold(I)-non-steroidal anti-inflammatory drug complexes. *Chem. Sci.* **2023**, *14*, 557.
(55) Cai, W.; Zhang, L.; Song, Y.; Wang, B.; Zhang, B.; Cui, X.; Hu, G.; Liu, Y.; Wu, J.; Fang, J. Small molecule inhibitors of mammalian thioredoxin reductase. *Free Radical Biol. Med.* **2012**, *52*, 257.
(56) Arnér, E. S. J. Focus on mammalian thioredoxin reductases - Important selenoproteins with versatile functions. *Biochim. Biophys. Acta* **2009**, *1790*, 495.
(57) Horstkotte, J.; Perisic, T.; Schneider, M.; Lange, P.; Schroeder, M.; Kiermayer, C.; Hinkel, R.; Ziegler, T.; Mandal, P. K.; David, R.; Schulz, S.; Schmitt, S.; Widder, J.; Sinowatz, F.; Becker, B. F.; Bauersachs, J.; Naebauer, M.; Franz, W. M.; Jeremias, I.; Brielmeier, M.; Zischka, H.; Conrad, M.; Kupatt, C. Mitochondrial Thioredoxin Reductase Is Essential for Early Postischemic Myocardial Protection. *Circulation* **2011**, *124*, 2892.
(58) Chocron, E. S.; Mdaki, K.; Jiang, N.; Cropper, J.; Pickering, A. M. Mitochondrial TrxR2 regulates metabolism and protects from metabolic disease through enhanced TCA and ETC function. *Commun. Biol.* **2022**, *5*, 467.
(59) Stafford, W. C.; Peng, X.; Olofsson, M. H.; Zhang, X.; Luci, D. K.; Lu, L.; Cheng, Q.; Trésaugues, L.; Dexheimer, T. S.; Coussens, N. P.; et al. Irreversible inhibition of cytosolic thioredoxin reductase 1 as a mechanistic basis for anticancer therapy. *Sci. Transl. Med.* **2018**, *10*, eaaf7444.
(60) Kameritsch, P.; Singer, M.; Nuernbergk, C.; Rios, N.; Reyes, A. M.; Schmidt, K.; Kirsch, J.; Schneider, H.; Müller, S.; Pogoda, K.; et al. The mitochondrial thioredoxin reductase system (TrxR2) in vascular endothelium controls peroxynitrite levels and tissue integrity. *Proc. Natl. Acad. Sci. USA* **2021**, *118*, e1921828118.
(61) Uhlen, M.; Zhang, C.; Lee, S.; Sjöstedt, E.; Fagerberg, L.; Bidkhori, G.; Benfeitas, R.; Arif, M.; Liu, Z.; Edfors, F.; et al. A pathology atlas of the human cancer transcriptome. *Science* **2017**, *357*, eaan2507.
(62) Berglund, L.; Björling, E.; Oksvold, P.; Fagerberg, L.; Asplund, A.; Al-Khalili Szigyarto, C.; Persson, A.; Ottosson, J.; Wernérus, H.; Nilsson, P.; Lundberg, E.; Sivertsson, Å.; Navani, S.; Wester, K.; Kampf, C.; Hober, S.; Pontén, F.; Uhlén, M. A Genecentric Human Protein Atlas for Expression Profiles Based on Antibodies. *Mol. Cell. Proteomics* **2008**, *7*, 2019.
(63) Tsherniak, A.; Vazquez, F.; Montgomery, P. G.; Weir, B. A.; Kryukov, G.; Cowley, G. S.; Gill, S.; Harrington, W. F.; Pantel, S.; Krill-Burger, J. M.; Meyers, R. M.; Ali, L.; Goodale, A.; Lee, Y.; Jiang, G.; Hsiao, J.; Gerath, W. F. J.; Howell, S.; Merkel, E.; Ghandi, M.; Garraway, L. A.; Root, D. E.; Golub, T. R.; Boehm, J. S.; Hahn, W. C. Defining a Cancer Dependency Map. *Cell* **2017**, *170*, 564.
(64) Bindoli, A.; Rigobello, M. P.; Scutari, G.; Gabbiani, C.; Casini, A.; Messori, L. Thioredoxin reductase: A target for gold compounds acting as potential anticancer drugs. *Coord. Chem. Rev.* **2009**, *253*, 1692.
(65) Jiang, J.; Xiong, X.; Zou, T. Modulating the Chemical Reactivity of Gold Complexes in Living Systems: From Concept to Biomedical Applications. *Acc. Chem. Res.* **2023**, *56*, 1043.
(66) Rajendran, L.; Knölker, H.-J.; Simons, K. Subcellular targeting strategies for drug design and delivery. *Nat. Rev. Drug Discovery* **2010**, *9*, 29.
(67) Lv, W.; Champion, J. A. Demonstration of intracellular trafficking, cytosolic bioavailability, and target manipulation of an antibody delivery platform. *Nanomed. Nanotechnol. Biol. Med.* **2021**, *32*, 102315.
(68) Watson, G. M.; Kulkarni, K.; Brandt, R.; Del Borgo, M. P.; Aguilar, M.-I.; Wilce, J. A. Shortened Penetratin Cell-Penetrating Peptide Is Insufficient for Cytosolic Delivery of a Grb7 Targeting Peptide. *ACS Omega* **2017**, *2*, 670.
(69) Yu, L.; Xu, Y.; Pu, Z.; Kang, H.; Li, M.; Sessler, J. L.; Kim, J. S. Photocatalytic Superoxide Radical Generator that Induces Pyroptosis in Cancer Cells. *J. Am. Chem. Soc.* **2022**, *144*, 11326.
(70) Su, X.; Wang, W.-J.; Cao, Q.; Zhang, H.; Liu, B.; Ling, Y.; Zhou, X.; Mao, Z.-W. A Carbonic Anhydrase IX (CAIX)-Anchored Rhenium(I) Photosensitizer Evokes Pyroptosis for Enhanced Anti-Tumor Immunity. *Angew. Chem., Int. Ed.* **2022**, *61*, e202115800.
(71) Yuan, H.; Han, Z.; Chen, Y.; Qi, F.; Fang, H.; Guo, Z.; Zhang, S.; He, W. Ferroptosis Photoinduced by New Cyclometalated Iridium(III) Complexes and Its Synergism with Apoptosis in Tumor Cell Inhibition. *Angew. Chem., Int. Ed.* **2021**, *60*, 8174.
(72) Zhou, X.-Q.; Wang, P.; Ramu, V.; Zhang, L.; Jiang, S.; Li, X.; Abyar, S.; Papadopoulou, P.; Shao, Y.; Bretin, L.; Siegler, M. A.; Buda, F.; Kros, A.; Fan, J.; Peng, X.; Sun, W.; Bonnet, S. In vivo metallophilic self-assembly of a light-activated anticancer drug. *Nat. Chem.* **2023**, *15*, 980−987.
(73) Wang, X.; Wang, X.; Jin, S.; Muhammad, N.; Guo, Z. Stimuli-Responsive Therapeutic Metallodrugs. *Chem. Rev.* **2019**, *119*, 1138.
(74) Imberti, C.; Zhang, P.; Huang, H.; Sadler, P. J. New Designs for Phototherapeutic Transition Metal Complexes. *Angew. Chem., Int. Ed.* **2020**, *59*, 61.
(75) Amarsy, I.; Papot, S.; Gasser, G. Stimuli-Responsive Metal Complexes for Biomedical Applications. *Angew. Chem., Int. Ed.* **2022**, *61*, e202205900.
(76) Zhang, Y.; Doan, B.-T.; Gasser, G. Metal-Based Photosensitizers as Inducers of Regulated Cell Death Mechanisms. *Chem. Rev.* **2023**, *123*, 10135.
(77) Bonnet, S. Ruthenium-Based Photoactivated Chemotherapy. *J. Am. Chem. Soc.* **2023**, *145*, 23397.
(78) Joshi, T.; Pierroz, V.; Mari, C.; Gemperle, L.; Ferrari, S.; Gasser, G. A Bis(dipyridophenazine)(2-(2-pyridyl)pyrimidine-4-carboxylic acid)ruthenium(II) Complex with Anticancer Action upon Photodeprotection. *Angew. Chem., Int. Ed.* **2014**, *53*, 2960.
(79) Knoll, J. D.; Albani, B. A.; Turro, C. New Ru(II) Complexes for Dual Photoreactivity: Ligand Exchange and $^1O_2$ Generation. *Acc. Chem. Res.* **2015**, *48*, 2280.
(80) Lameijer, L. N.; Ernst, D.; Hopkins, S. L.; Meijer, M. S.; Askes, S. H. C.; Le Dévédec, S. E.; Bonnet, S. A Red-Light-Activated Ruthenium-Caged NAMPT Inhibitor Remains Phototoxic in Hypoxic Cancer Cells. *Angew. Chem., Int. Ed.* **2017**, *56*, 11549.
(81) Li, A.; Turro, C.; Kodanko, J. J. Ru(II) polypyridyl complexes as photocages for bioactive compounds containing nitriles and aromatic heterocycles. *Chem. Commun.* **2018**, *54*, 1280.
(82) van Rixel, V. H. S.; Ramu, V.; Auyeung, A. B.; Beztsinna, N.; Leger, D. Y.; Lameijer, L. N.; Hilt, S. T.; Le Dévédec, S. E.; Yildiz, T.; Betancourt, T.; Gildner, M. B.; Hudnall, T. W.; Sol, V.; Liagre, B.; Kornienko, A.; Bonnet, S. Photo-Uncaging of a Microtubule-Targeted Rigidin Analogue in Hypoxic Cancer Cells and in a Xenograft Mouse Model. *J. Am. Chem. Soc.* **2019**, *141*, 18444.
(83) van Rixel, V. H. S.; Busemann, A.; Wissingh, M. F.; Hopkins, S. L.; Siewert, B.; van de Griend, C.; Siegler, M. A.; Marzo, T.; Papi, F.; Ferraroni, M.; Gratteri, P.; Bazzicalupi, C.; Messori, L.; Bonnet, S. Induction of a Four-Way Junction Structure in the DNA Palindromic Hexanucleotide 5′-d(CGTACG)-3′ by a Mononuclear Platinum Complex. *Angew. Chem., Int. Ed.* **2019**, *58*, 9378.
(84) Toupin, N.; Steinke, S. J.; Nadella, S.; Li, A.; Rohrabaugh, T. N., Jr.; Samuels, E. R.; Turro, C.; Sevrioukova, I. F.; Kodanko, J. J. Photosensitive Ru(II) Complexes as Inhibitors of the Major Human

https://doi.org/10.1021/jacs.5c03186
J. Am. Chem. Soc. 2025, 147, 15719−15731

Drug Metabolizing Enzyme CYP3A4. *J. Am. Chem. Soc.* **2021**, *143*, 9191.
(85) Steinke, S. J.; Gupta, S.; Piechota, E. J.; Moore, C. E.; Kodanko, J. J.; Turro, C. Photocytotoxicity and photoinduced phosphine ligand exchange in a Ru(II) polypyridyl complex. *Chem. Sci.* **2022**, *13*, 1933.
(86) Lai, Y.; Lu, N.; Luo, S.; Wang, H.; Zhang, P. A Photoactivated Sorafenib-Ruthenium(II) Prodrug for Resistant Hepatocellular Carcinoma Therapy through Ferroptosis and Purine Metabolism Disruption. *J. Med. Chem.* **2022**, *65*, 13041.
(87) Steinke, S. J.; Piechota, E. J.; Loftus, L. M.; Turro, C. Acetonitrile Ligand Photosubstitution in Ru(II) Complexes Directly from the 3MLCT State. *J. Am. Chem. Soc.* **2022**, *144*, 20177.
(88) Hakkennes, M. L. A.; Meijer, M. S.; Menzel, J. P.; Goetz, A.-C.; Van Duijn, R.; Siegler, M. A.; Buda, F.; Bonnet, S. Ligand Rigidity Steers the Selectivity and Efficiency of the Photosubstitution Reaction of Strained Ruthenium Polypyridyl Complexes. *J. Am. Chem. Soc.* **2023**, *145*, 13420.
(89) Ballester, F. J.; Hernández-García, A.; Santana, M. D.; Bautista, D.; Ashoo, P.; Ortega-Forte, E.; Barone, G.; Ruiz, J. Photoactivatable Ruthenium Complexes Containing Minimal Straining Benzothiazolyl-1,2,3-triazole Chelators for Cancer Treatment. *Inorg. Chem.* **2024**, *63*, 6202.
(90) Farrer, N. J.; Woods, J. A.; Salassa, L.; Zhao, Y.; Robinson, K. S.; Clarkson, G.; Mackay, F. S.; Sadler, P. J. A Potent Trans-Diimine Platinum Anticancer Complex Photoactivated by Visible Light. *Angew. Chem., Int. Ed.* **2010**, *49*, 8905.
(91) Alonso-de Castro, S.; Ruggiero, E.; Ruiz-de-Angulo, A.; Rezabal, E.; Mareque-Rivas, J. C.; Lopez, X.; López-Gallego, F.; Salassa, L. Riboflavin as a bioorthogonal photocatalyst for the activation of a PtIV prodrug. *Chem. Sci.* **2017**, *8*, 4619.
(92) Alonso-de Castro, S.; Cortajarena, A. L.; López-Gallego, F.; Salassa, L. Bioorthogonal Catalytic Activation of Platinum and Ruthenium Anticancer Complexes by FAD and Flavoproteins. *Angew. Chem., Int. Ed.* **2018**, *57*, 3143.
(93) Wang, Z.; Wang, N.; Cheng, S.-C.; Xu, K.; Deng, Z.; Chen, S.; Xu, Z.; Xie, K.; Tse, M.-K.; Shi, P.; Hirao, H.; Ko, C.-C.; Zhu, G. Phorbiplatin, a Highly Potent Pt(IV) Antitumor Prodrug That Can Be Controllably Activated by Red Light. *Chem.* **2019**, *5*, 3151.
(94) Deng, Z.; Wang, N.; Liu, Y.; Xu, Z.; Wang, Z.; Lau, T.-C.; Zhu, G. A Photocaged, Water-Oxidizing, and Nucleolus-Targeted Pt(IV) Complex with a Distinct Anticancer Mechanism. *J. Am. Chem. Soc.* **2020**, *142*, 7803.
(95) Bolitho, E. M.; Sanchez-Cano, C.; Shi, H.; Quinn, P. D.; Harkiolaki, M.; Imberti, C.; Sadler, P. J. Single-Cell Chemistry of Photoactivatable Platinum Anticancer Complexes. *J. Am. Chem. Soc.* **2021**, *143*, 20224.
(96) Velasco-Lozano, S.; Castro, S. A. -d.; Sanchez-Cano, C.; Benítez-Mateos, A. I.; López-Gallego, F.; Salassa, L. Metal substrate catalysis in the confined space for platinum drug delivery. *Chem. Sci.* **2021**, *13*, 59.
(97) Kastl, A.; Wilbuer, A.; Merkel, A. L.; Feng, L.; Di Fazio, P.; Ocker, M.; Meggers, E. Dual anticancer activity in a single compound: visible-light-induced apoptosis by an antiangiogenic iridium complex. *Chem. Commun.* **2012**, *48*, 1863.
(98) Kuang, S.; Wei, F.; Karges, J.; Ke, L.; Xiong, K.; Liao, X.; Gasser, G.; Ji, L.; Chao, H. Photodecaging of a Mitochondria-Localized Iridium(III) Endoperoxide Complex for Two-Photon Photoactivated Therapy under Hypoxia. *J. Am. Chem. Soc.* **2022**, *144*, 4091.
(99) Yip, A. M.-H.; Lai, C. K.-H.; Yiu, K. S.-M.; Lo, K. K.-W. Phosphorogenic Iridium(III) bis-Tetrazine Complexes for Bioorthogonal Peptide Stapling, Bioimaging, Photocytotoxic Applications, and the Construction of Nanosized Hydrogels. *Angew. Chem., Int. Ed.* **2022**, *61*, e202116078.
(100) Liu, M.; Luo, Y.; Yan, J.; Xiong, X.; Xing, X.; Kim, J. S.; Zou, T. Photoactivation of Boronic Acid Prodrugs via a Phenyl Radical Mechanism: Iridium(III) Anticancer Complex as an Example. *J. Am. Chem. Soc.* **2023**, *145*, 10082.
(101) Luo, H.; Cao, B.; Chan, A. S. C.; Sun, R. W.-Y.; Zou, T. Cyclometalated Gold(III)-Hydride Complexes Exhibit Visible Light-Induced Thiol Reactivity and Act as Potent Photo-Activated Anti-Cancer Agents. *Angew. Chem., Int. Ed.* **2020**, *59*, 11046.
(102) Li, Z.; David, A.; Albani, B. A.; Pellois, J.-P.; Turro, C.; Dunbar, K. R. Optimizing the Electronic Properties of Photoactive Anticancer Oxypyridine-Bridged Dirhodium(II,II) Complexes. *J. Am. Chem. Soc.* **2014**, *136*, 17058.
(103) Garai, A.; Pant, I.; Banerjee, S.; Banik, B.; Kondaiah, P.; Chakravarty, A. R. Photorelease and Cellular Delivery of Mitocurcumin from Its Cytotoxic Cobalt(III) Complex in Visible Light. *Inorg. Chem.* **2016**, *55*, 6027.
(104) Askes, S. H. C.; Reddy, G. U.; Wyrwa, R.; Bonnet, S.; Schiller, A. Red Light-Triggered CO Release from $Mn_2(CO)_{10}$ Using Triplet Sensitization in Polymer Nonwoven Fabrics. *J. Am. Chem. Soc.* **2017**, *139*, 15292.
(105) Marco, A.; Ashoo, P.; Hernández-García, S.; Martínez-Rodríguez, P.; Cutillas, N.; Vollrath, A.; Jordan, D.; Janiak, C.; Gandía-Herrero, F.; Ruiz, J. Novel Re(I) Complexes as Potential Selective Theranostic Agents in Cancer Cells and In Vivo in *Caenorhabditis elegans* Tumoral Strains. *J. Med. Chem.* **2024**, *67*, 7891.
(106) Demartis, S.; Anjani, Q. K.; Volpe-Zanutto, F.; Paredes, A. J.; Jahan, S. A.; Vora, L. K.; Donnelly, R. F.; Gavini, E. Trilayer dissolving polymeric microneedle array loading Rose Bengal transfersomes as a novel adjuvant in early-stage cutaneous melanoma management. *Int. J. Pharm.* **2022**, *627*, 122217.
(107) Hamid, O.; Ismail, R.; Puzanov, I. Intratumoral Immunotherapy—Update 2019. *Oncologist* **2020**, *25*, e423.
(108) Qin, J.; Kunda, N.; Qiao, G.; Calata, J. F.; Pardiwala, K.; Prabhakar, B. S.; Maker, A. V. Colon cancer cell treatment with rose bengal generates a protective immune response via immunogenic cell death. *Cell Death & Disease* **2017**, *8*, No. e2584.
(109) Khdair, A.; Gerard, B.; Handa, H.; Mao, G.; Shekhar, M. P. V.; Panyam, J. Surfactant−Polymer Nanoparticles Enhance the Effectiveness of Anticancer Photodynamic Therapy. *Mol. Pharmaceutics* **2008**, *5*, 795.
(110) Mellish, K. J.; Cox, R. D.; Vernon, D. I.; Griffiths, J.; Brown, S. B. In Vitro Photodynamic Activity of a Series of Methylene Blue Analogues. *Photochem. Photobiol.* **2002**, *75*, 392.
(111) Berg, K.; Selbo, P. K.; Prasmickaite, L.; Tjelle, T. E.; Sandvig, K.; Moan, J.; Gaudernack, G.; Fodstad, Ø.; Kjølsrud, S.; Anholt, H.; Rodal, G. H.; Rodal, S. K.; Høgset, A. Photochemical Internalization: A Novel Technology for Delivery of Macromolecules into Cytosol. *Cancer Res.* **1999**, *59*, 1180.
(112) Zhang, Q.; Cai, Y.; Li, Q.-Y.; Hao, L.-N.; Ma, Z.; Wang, X.-J.; Yin, J. Targeted Delivery of a Mannose-Conjugated BODIPY Photosensitizer by Nanomicelles for Photodynamic Breast Cancer Therapy. *Chem.—Eur. J.* **2017**, *23*, 14307.
(113) Yang, Y.; Ning, H.; Xia, T.; Du, J.; Sun, W.; Fan, J.; Peng, X. Electrostatic Attractive Self-Delivery of siRNA and Light-Induced Self-Escape for Synergistic Gene Therapy. *Adv. Mater.* **2023**, *35*, 2301409.
(114) Xue, X.; Qian, C.; Fang, H.; Liu, H.-K.; Yuan, H.; Guo, Z.; Bai, Y.; He, W. Photoactivated Lysosomal Escape of a Monofunctional PtII Complex Pt-BDPA for Nucleus Access. *Angew. Chem., Int. Ed.* **2019**, *58*, 12661.
(115) Xie, Z.; Cao, B.; Zhao, J.; Liu, M.; Lao, Y.; Luo, H.; Zhong, Z.; Xiong, X.; Wei, W.; Zou, T. Ion Pairing Enables Targeted Prodrug Activation via Red Light Photocatalysis: A Proof-of-Concept Study with Anticancer Gold Complexes. *J. Am. Chem. Soc.* **2024**, *146*, 8547.
(116) Liu, Z.; Xie, X.; Huang, Z.; Lin, F.; Liu, S.; Chen, Z.; Qin, S.; Fan, X.; Chen, P. R. Spatially resolved cell tagging and surfaceome labeling via targeted photocatalytic decaging. *Chem.* **2022**, *8*, 2179.
(117) Bloom, S.; Liu, C.; Kölmel, D. K.; Qiao, J. X.; Zhang, Y.; Poss, M. A.; Ewing, W. R.; MacMillan, D. W. C. Decarboxylative alkylation for site-selective bioconjugation of native proteins via oxidation potentials. *Nat. Chem.* **2018**, *10*, 205.
(118) Cabanero, D. C.; Kariofillis, S. K.; Johns, A. C.; Kim, J.; Ni, J.; Park, S.; Parker, D. L., Jr.; Ramil, C. P.; Roy, X.; Shah, N. H.; Rovis, T.

https://doi.org/10.1021/jacs.5c03186
J. Am. Chem. Soc. 2025, 147, 15719−15731

Photocatalytic Activation of Aryl(trifluoromethyl) Diazos to Carbenes for High-Resolution Protein Labeling with Red Light. *J. Am. Chem. Soc.* **2024**, *146*, 1337.
(119) D'Avino, C.; Gutiérrez, S.; Feldhaus, M. J.; Tomás-Gamasa, M.; Mascareñas, J. L. Intracellular Synthesis of Indoles Enabled by Visible-Light Photocatalysis. *J. Am. Chem. Soc.* **2024**, *146*, 2895.
(120) Goetzfried, S. K.; Gallati, C. M.; Cziferszky, M.; Talmazan, R. A.; Wurst, K.; Liedl, K. R.; Podewitz, M.; Gust, R. N-Heterocyclic Carbene Gold(I) Complexes: Mechanism of the Ligand Scrambling Reaction and Their Oxidation to Gold(III) in Aqueous Solutions. *Inorg. Chem.* **2020**, *59*, 15312.
(121) Schmidt, C.; Albrecht, L.; Balasupramaniam, S.; Misgeld, R.; Karge, B.; Brönstrup, M.; Prokop, A.; Baumann, K.; Reichl, S.; Ott, I. A gold(I) biscarbene complex with improved activity as a TrxR inhibitor and cytotoxic drug: comparative studies with different gold metallodrugs. *Metallomics* **2019**, *11*, 533.
(122) Karaca, Ö.; Scalcon, V.; Meier-Menches, S. M.; Bonsignore, R.; Brouwer, J. M. J. L.; Tonolo, F.; Folda, A.; Rigobello, M. P.; Kühn, F. E.; Casini, A. Characterization of Hydrophilic Gold(I) N-Heterocyclic Carbene (NHC) Complexes as Potent TrxR Inhibitors Using Biochemical and Mass Spectrometric Approaches. *Inorg. Chem.* **2017**, *56*, 14237.
(123) Liu, D.-Y.; Han, J.; Liu, K.; Cheng, Y.; Tan, H.; Yang, X.; Li, W.; Xie, J. Dinuclear Gold-Catalyzed para-Selective C−H Arylation of Undirected Arenes by Noncovalent Interactions. *Angew. Chem., Int. Ed.* **2023**, *62*, e202313122.
(124) Leyva-Pérez, A.; Doménech-Carbó, A.; Corma, A. Unique distal size selectivity with a digold catalyst during alkyne homocoupling. *Nat. Commun.* **2015**, *6*, 6703.
(125) Peng, H.; Xi, Y.; Ronaghi, N.; Dong, B.; Akhmedov, N. G.; Shi, X. Gold-Catalyzed Oxidative Cross-Coupling of Terminal Alkynes: Selective Synthesis of Unsymmetrical 1,3-Diynes. *J. Am. Chem. Soc.* **2014**, *136*, 13174.
(126) Compound **1a** cannot be washed since it can freely cross the cell membrane. The cell-based experiments using the similar procedure but without the PC removing step have been carried out, showing similar results (Figure S29)
(127) Wei, W.; Zhu, T.; Wang, Y.; Yang, H.; Hao, Z.; Chen, P. R.; Zhao, J. Engineering a gold-specific regulon for cell-based visual detection and recovery of gold. *Chem. Sci.* **2012**, *3*, 1780.
(128) Weiss, J. T.; Dawson, J. C.; Macleod, K. G.; Rybski, W.; Fraser, C.; Torres-Sánchez, C.; Patton, E. E.; Bradley, M.; Carragher, N. O.; Unciti-Broceta, A. Extracellular palladium-catalysed dealkylation of 5-fluoro-1-propargyl-uracil as a bioorthogonally activated prodrug approach. *Nat. Commun.* **2014**, *5*, 3277.
(129) Vidal, C.; Tomás-Gamasa, M.; Destito, P.; López, F.; Mascareñas, J. L. Concurrent and orthogonal gold(I) and ruthenium-(II) catalysis inside living cells. *Nat. Commun.* **2018**, *9*, 1913.
(130) Latocheski, E.; Dal Forno, G. M.; Ferreira, T. M.; Oliveira, B. L.; Bernardes, G. J. L.; Domingos, J. B. Mechanistic insights into transition metal-mediated bioorthogonal uncaging reactions. *Chem. Soc. Rev.* **2020**, *49*, 7710.
(131) Oliveira, B. L.; Stenton, B. J.; Unnikrishnan, V. B.; de Almeida, C. R.; Conde, J.; Negrão, M.; Schneider, F. S. S.; Cordeiro, C.; Ferreira, M. G.; Caramori, G. F.; Domingos, J. B.; Fior, R.; Bernardes, G. J. L. Platinum-Triggered Bond-Cleavage of Pentynoyl Amide and N-Propargyl Handles for Drug-Activation. *J. Am. Chem. Soc.* **2020**, *142*, 10869.
(132) You, Y.; Deng, Q.; Wang, Y.; Sang, Y.; Li, G.; Pu, F.; Ren, J.; Qu, X. DNA-based platform for efficient and precisely targeted bioorthogonal catalysis in living systems. *Nat. Commun.* **2022**, *13*, 1459.
(133) Vanjari, R.; Panda, D.; Mandal, S.; Vamisetti, G. B.; Brik, A. Gold(I)-Mediated Rapid Cyclization of Propargylated Peptides via Imine Formation. *J. Am. Chem. Soc.* **2022**, *144*, 4966.
(134) Gutiérrez, S.; Tomás-Gamasa, M.; Mascareñas, J. L. Exporting Metal-Carbene Chemistry to Live Mammalian Cells: Copper-Catalyzed Intracellular Synthesis of Quinoxalines Enabled by N−H Carbene Insertions. *Angew. Chem., Int. Ed.* **2021**, *60*, 22017.
(135) Huang, Z.; Liu, Z.; Xie, X.; Zeng, R.; Chen, Z.; Kong, L.; Fan, X.; Chen, P. R. Bioorthogonal Photocatalytic Decaging-Enabled Mitochondrial Proteomics. *J. Am. Chem. Soc.* **2021**, *143*, 18714.
(136) Zhao, Z.; Li, J.; Yuan, W.; Cheng, D.; Ma, S.; Li, Y.-F.; Shi, Z.-J.; Hu, K. Nature-Inspired Photocatalytic Azo Bond Cleavage with Red Light. *J. Am. Chem. Soc.* **2024**, *146*, 1364.
(137) Liu, Y.; Ma, H.; Zhang, L.; Cui, Y.; Liu, X.; Fang, J. A small molecule probe reveals declined mitochondrial thioredoxin reductase activity in a Parkinson's disease model. *Chem. Commun.* **2016**, *52*, 2296.
(138) Glover, H. L.; Schreiner, A.; Dewson, G.; Tait, S. W. G. Mitochondria and cell death. *Nat. Cell Biol.* **2024**, *26*, 1434−1446.
(139) He, C.; Bartholomew, C. R.; Zhou, W.; Klionsky, D. J. Assaying autophagic activity in transgenic GFP-Lc3 and GFP-Gabarap zebrafish embryos. *Autophagy* **2009**, *5*, 520.
(140) Dhillon, S. K.; Porter, S. L.; Rizk, N.; Sheng, Y.; McKaig, T.; Burnett, K.; White, B.; Nesbitt, H.; Matin, R. N.; McHale, A. P.; Callan, B.; Callan, J. F. Rose Bengal−Amphiphilic Peptide Conjugate for Enhanced Photodynamic Therapy of Malignant Melanoma. *J. Med. Chem.* **2020**, *63*, 1328.
(141) Zhao, J.; Yang, Y.; Xu, X.; Li, H.; Fei, J.; Liu, Y.; Zhang, X.; Li, J. Super Light-Sensitive Photosensitizer Nanoparticles for Improved Photodynamic Therapy against Solid Tumors. *Angew. Chem., Int. Ed.* **2022**, *61*, e202210920.

https://doi.org/10.1021/jacs.5c03186
J. Am. Chem. Soc. 2025, 147, 15719−15731